Available online at www.sciencedirect.com
ScienceDirect
Trans. Nonferrous Met. Soc. China 26(2016) 1044−1054
Transactions of Nonferrous Metals Society of China
www.tnmsc.cn

Effect of strain rate and deformation temperature on strain hardening and softening behavior of pure copper

Shu-hai HUANG, Da-yu SHU, Chuan-kai HU, Shi-feng ZHU

Southwest Technique and Engineering Institute, Chongqing 400039, China

Received 21 April 2015; accepted 3 December 2015

Abstract: The effects of the deformation temperature and the strain rate on the hot deformation behavior of pure copper were investigated based on compression tests. The expressions of strain hardening rate, dynamic recrystallization critical stress, saturated stress, dynamic recovery volume fraction and dynamic recrystallization volume fraction were determined. According to the processing map, the instability regions occur in regions of 400−450 °C, 0.001−0.05 s^{-1} and 450−750 °C, 0.05−1 s^{-1}. The deformation mechanism in the stability region is dynamic recrystallization. The flow stress was predicted. The results also show that the true stress–true strain curves predicted by the extracted model are in good agreement with the experimental results.
Key words: copper; hot compression deformation; strain hardening; strain softening

1 Introduction

Pure copper cartridge receivers with complex geometries used in the ordnance industry are generally manufactured at high temperatures and very low strain rates due to the strict requirement of the fine-grained structure. Forging at high temperatures is widely used to obtain copper parts with complex shapes. Therefore, to optimize the fabrication process, it is necessary to study the hot deformation behavior of pure copper at high temperatures and low strain rates. Hot deformation behavior is often simulated by compression tests due to their similarity to forging processes. When pure copper is compressed at high temperatures, the flow stress curves present three typical regions of hot deformation: a strain hardening (SH) region characterized by an increasing dislocation density, followed by a dynamic recovery (DRV) characterized by polygonal sub-grain structures, and finally dynamic recrystallization (DRX) in which build-up of dislocations leads to nucleation and growth of DRX grains during the deformation process until a steady state is reached [1−3].

The hot deformation behaviors of nonferrous metals, such as constitutive equations, prediction of flow stress, flow softening behaviors, mainly focused on aluminum alloys, magnesium alloys and titanium alloys [4−7]; however, investigations on strain hardening and softening behaviors of pure copper are very rare. GRONOSTAJSKI [8] proposed a general model to describe the flow stress as a function of the internal state of copper alloys. The model described strain hardening and dynamic softening processes taking place during the deformation process or static softening during interval or after deformation. MANONUKUL and DUNNE [9] established a hot deformation model of pure copper. The model was calibrated using the homogeneous test data and used to predict the deformation, the initiation of DRX, and the microstructural change in the truncated cone specimens. After comparing the computed results with the experimental results, the model was proven to be capable of tracking the motion of recrystallization fronts through the deforming material under conditions of inhomogeneous stresses. PRASAD and RAO [10] studied mechanisms of high temperature deformation in electrolytic copper in extended ranges of temperature and strain rate. The switching of the rate controlling mechanisms at 700 °C was attributed to the “clogging” of the dislocation pipes due to the rapid increase in the solid solubility of oxygen at high temperatures.

The aim of this work is to study the effects of strain rate and deformation temperature on strain hardening and softening behaviors of pure copper. Therefore, we can gain a better understanding of hot forging for pure

Foundation item: Project (cstc2015jcyjBX0115) supported by the Chongqing Research Program of Basic Research and Frontier Technology, China
Corresponding author: Shu-hai HUANG; Tel: +86-13678486826; Fax: +86-23-68792232; E-mail: hsh82@163.com
DOI: 10.1016/S1003-6326(16)64201-2

copper cartridge receivers with complex geometries.

2 Experimental

The material used in this work was pure copper bar, which was annealed at 420 °C for 2 h. Cylindrical specimens with 12 mm in height and 8 mm in diameter were cut from the annealed bar, and the initial average size was about 180 μm. Compression test was carried out on a Gleeble−1500 thermal simulator in the temperature range of 400−900 °C and strain rate range of 0.001−1 s^{-1}. The total compression deformation was 60%. The whole compression process was controlled by a computer capable of collecting relevant data in an automatic way.

Figure 1 shows the stress−strain curves of pure copper under different conditions. Typically, the flow stress decreases with increasing the temperature and decreasing the strain rate. When the deformation temperature is comparatively low, strain hardening dominates the deformation, which is more apparent in the high strain rate region. After peak strain, the flow stress decreases with the increase of strain; with further

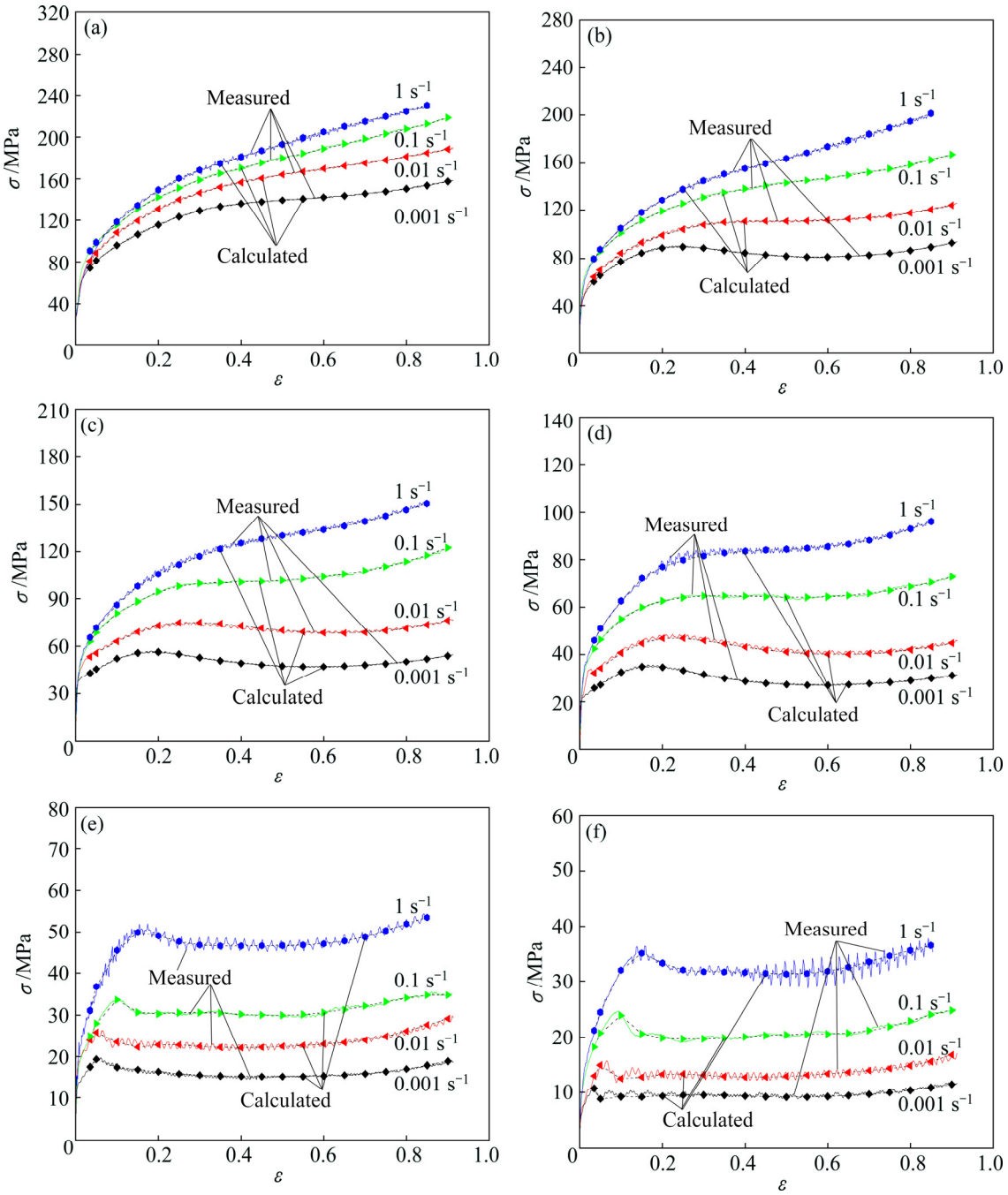

Fig. 1 Stress−strain curves of pure copper at different strain rates and temperatures: (a) 400 °C; (b) 500 °C; (c) 600 °C; (d) 700 °C; (e) 800 °C; (f) 900 °C

increase in the strain, the secondary strain hardening takes place. Compared with the first strain hardening rate, the secondary hardening rate is much lower. The shape of the stress−strain curves can reflect the mechanisms of hot deformation. For example, the flow stress increases with increasing the strain in the initial stage of deformation, which is always caused by the strain hardening. Then, the flow stress decreases due to the dynamic recrystallization or recovery processes. Detailed analysis about the hot deformation mechanism will be carried out in the subsequent discussion.

3 Principles of strain hardening and softening

During thermoplastic deformation, the variation of flow stress is generally determined by strain hardening and softening [11−14]. Plastic deformation is primarily completed by dislocation movement, multiplication and annihilation. The dislocation density increases with the increase of strain, resulting in the strain hardening. There are two kinds of mechanisms of strain softening: dynamic recovery and dynamic recrystallization. The behavior of flow stress can be roughly divided into three stages (Fig. 2). Firstly, before strain ε reaches the initial yield strain, ε_0, i.e., $\varepsilon<\varepsilon_0$, the elastic deformation of materials is dominant. Secondly, before the strain ε approaches the critical strain ε_c of dynamic recrystallization, i.e., $\varepsilon_0<\varepsilon<\varepsilon_c$, plastic deformation of materials takes place. In this situation, strain hardening and dynamic recovery are dominant. At last, when the strain ε reaches an steady state deformation ε_{ss}, i.e., $\varepsilon_c<\varepsilon<\varepsilon_{ss}$, strain hardening, dynamic recovery and dynamic recrystallization softening occur alternately with the increase of the deformation degree. Peak strain ε_p can be considered as the initial point of the balance that is achieved between the strain hardening posed by dislocation pile-up and the recovery softening resulted from the dynamic recrystallization. Assuming that there is no dynamic recrystallization during deformation and only the strain hardening and the dynamic recovery are available, the dynamic recovery stress (σ_{rec}) curve may be obtained by calculation. σ_{sat} is the asymptotic stress under the state of saturated stress.

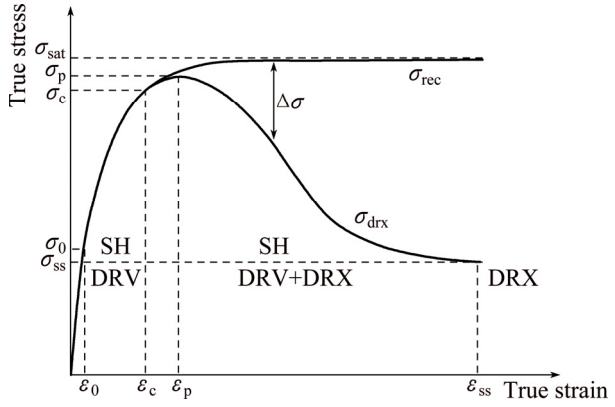

Fig. 2 Schematic diagram of thermoplastic deformation stress−strain curve

3.1 Modeling strain hardening and dynamic recovery

When the deformed material turns into the state of yield, the plastic deformation of materials becomes obvious. A large number of dislocation movements take place inside the materials. Consequently, interactions including initiation of fixed dislocation movement, dislocation multiplication, annihilation and rearrangement are enhanced. Dislocation density, ρ, is primarily determined by the increased dislocation density induced by the strain hardening during the deformation, while the reduced dislocation density is resulted from the dynamic recovery [11−13]. The dynamic recovery stress σ_{rec} of the material can be written as

$$\sigma_{rec}=\{\sigma_{sat}^2-(\sigma_{sat}^2-\sigma_0^2)\exp[-r(\varepsilon-\varepsilon_0)]\}^{1/2} \quad (1)$$

where σ_0 is the yield stress, ε_0 is the initial yield deformation, and r is the parameter of DRV.

3.2 Modeling dynamic recrystallization critical deformation

In the modern theory of dynamic recrystallization, the relation of $\varepsilon_c=\alpha_D\varepsilon_p$ is generally used to determine the critical strain ε_c of dynamic recrystallization, where α_D is the constant parameter. In the process of hot deformation of pure copper, various interactions of dislocation mechanisms, hardening, softening, diffusion activation and effective stress constitute a compound movement of dislocation during the deformation. Thus, it is difficult to accurately describe the critical condition of dynamic recrystallization occurring in the pure copper using a simple relationship between the critical strain ε_c and the peak strain ε_p. Accordingly, in this work, the incremental power balance method of the thermodynamic system was adopted to investigate the critical condition of dynamic recrystallization [15−17]:

$$\theta=\left.\frac{\mathrm{d}\sigma}{\mathrm{d}\varepsilon}\right|_{\dot{\varepsilon},T} \quad (2)$$

$$\frac{\mathrm{d}}{\mathrm{d}\sigma}\left(-\frac{\mathrm{d}\theta}{\mathrm{d}\sigma}\right)=0 \quad (3)$$

where θ is the strain hardening rate, and the critical strain ε_c is determined through the strain hardening rate θ on the flow curve and the inflection point on the flow stress σ curve or minimum value of $(-\mathrm{d}\theta/\mathrm{d}\sigma)$ on σ curve. In the actual investigation, a logarithmic relation is mostly used to describe the flow stress σ, which can be derived to be:

$$\theta = \sigma \cdot \frac{\mathrm{d}\ln\sigma}{\mathrm{d}\varepsilon} \tag{4}$$

$$-\frac{\mathrm{d}\theta}{\mathrm{d}\sigma} = -\left(\frac{\mathrm{d}\ln\sigma}{\mathrm{d}\varepsilon} + \frac{\mathrm{d}(\mathrm{d}\ln\sigma/\mathrm{d}\varepsilon)/\mathrm{d}\varepsilon}{\mathrm{d}\ln\sigma/\mathrm{d}\varepsilon}\right) \tag{5}$$

$$\frac{\mathrm{d}\ln\theta}{\mathrm{d}\varepsilon} = \frac{\mathrm{d}\theta}{\mathrm{d}\sigma} \tag{6}$$

3.3 Dynamic material modeling

Dynamic material modeling (DMM) is established based on the basic principles of large plastic deformation continuum mechanics, physical system simulation and irreversible thermodynamics. By determination of the parameters of the metal plastic deformation under different deformation conditions, features of power dissipation of the materials during plastic deformation are calculated, which can accurately describe the relationship between microstructural evolution of the metal at high temperature deformation and the plastic deformation parameters [18−21]. Under the condition of a given strain ε and the deformation temperature T, the strain rate sensitivity exponent m can be defined by the ratio of the change of the dissipation co-function J to the dissipation amount function G, as shown in Eq. (7):

$$m = \frac{\mathrm{d}J}{\mathrm{d}G} = \left[\frac{\partial\ln\sigma}{\partial\ln\dot{\varepsilon}}\right]_{\varepsilon,T} \tag{7}$$

The dimensionless power dissipation efficiency factor, η, can be described by the strain rate sensitivity exponent m, as shown in Eq. (8). To ensure the accuracy of m, a cubic equation function is generally used to fit the relationship between the flow stress $\ln\sigma$ and $\ln\dot{\varepsilon}$. Power dissipation efficiency factor, η, constitutes the power dissipation map with variations of temperature and strain rate.

$$\eta = \frac{J}{J_{\max}} = \frac{2m}{m+1} \tag{8}$$

According to the principle of irreversible thermodynamics, dimensionless parameter $\xi(\dot{\varepsilon})$ can be used to express the continuous instability criterion at large plastic deformations, as shown in Eq. (9). With the deformation temperature T and the strain rate $\dot{\varepsilon}$ as variables, the non-steady flow region with parameter $\xi(\dot{\varepsilon})$ smaller than zero constitutes the instability map.

$$\xi(\dot{\varepsilon}) = \frac{\partial\ln\left(\frac{m}{m+1}\right)}{\partial\ln\dot{\varepsilon}} + m < 0 \tag{9}$$

The power dissipation map and the instability map are superimposed to form DMM processing map corresponding to different true strain capacities, ε, where the shadow area is generally expressed as the instability region, and the digital on the equivalent line represents the power dissipation factor.

4 Results and discussion

4.1 Flow stress and thermal activation energy

Equation (10) is usually used to express the effect of the deformation extent on the flow stress [22,23]. It is found that when the strain rate $\dot{\varepsilon}$ and deformation temperature T are constant, the flow stress σ of pure copper and strain ε conform to the relation of Eq. (11). The calculated stress is in good agreement with the actual stress (Fig. 1).

$$\sigma = f_1(\dot{\varepsilon},T)f(\varepsilon) \tag{10}$$

$$\ln\sigma = a_0 + a_1\varepsilon + a_2\ln\varepsilon + a_3\varepsilon\ln\varepsilon + a_4\varepsilon^2\ln\varepsilon + a_5\varepsilon\ln\varepsilon^2 + a_6\varepsilon^2 + a_7\ln\varepsilon^2 + a_8\varepsilon^3 + a_9\ln\varepsilon^3 \tag{11}$$

where a_0−a_9 are constants, which can be determined by curve fitting. The peak stress σ_p and its corresponding peak strain ε_p decrease with elevating the deformation temperature and decreasing the strain rate concluded from the analysis of the flow stress curve. This is due to the fact that the recrystallization nucleation takes a longer time at a comparatively low strain rate, and the number of the nucleation increases to make the effect of recrystallization softening stronger than that of the strain hardening. At relatively high deformation temperature, the slip critical resolved shear stress (CRSS) decreases, and the dynamic recovery and dynamic recrystallization lead to reduced dislocation density, which make the peak stress occur in advance at the elevated temperatures. One of the features of the high temperature plastic deformation is that the strain rate is controlled by the thermal activation process. The effect of deformation temperature and strain rate on the flow stress of metal materials can be quantitatively expressed by the following creep equations [24,25]:

$$A_1\sigma^n = \dot{\varepsilon}\exp\left(\frac{Q}{RT}\right) = Z \tag{12}$$

$$A_2\exp(\beta\sigma) = \dot{\varepsilon}\exp\left(\frac{Q}{RT}\right) = Z \tag{13}$$

$$A[\sinh(\alpha\sigma)]^{n'} = \dot{\varepsilon}\exp\left(\frac{Q}{RT}\right) = Z \tag{14}$$

where Z is the Zener−Hollomon parameter, with the physical meaning of temperature compensated strain rate factors, s^{-1}; A_1, A_2, A, n, β, α and n' are constants independent of temperature, $\beta=\alpha n$; σ is the high temperature flow peak stress; $\dot{\varepsilon}$ is the strain rate, s^{-1}; T is the deformation temperature, K; R is the molar gas constant, 8.314 J/(mol·K); Q is the hot deformation activation energy, which reflects the difficulty level of

hot deformation of materials, kJ/mol. We found that Eqs. (12) and (13) are applicable to low stress deformation and high stress deformation, respectively. Equation (14) is the general form of Eqs. (12) and (13). In the case of $\alpha\sigma$<0.8, Eq. (14) can be simplified as Eq. (12), while when $\alpha\sigma$>1.2, Eq. (14) can be simplified as Eq. (13).

When deformation temperature T or strain rate $\dot{\varepsilon}$ is constant, peak stress σ_p exhibits a nearly linear relation with the logarithmic value of strain rate $\dot{\varepsilon}$ or the reciprocal value of temperature, as shown in Fig. 3. It can be seen that the pure copper is in agreement with the Arrhenius equation. For β value, the average value of the last three straight slopes in Fig. 3(a) is taken to obtain β=0.1154 MPa^{-1}. For n value, the average value of the former four straight slopes in Fig. 3(b) is taken to get the n value of 6.7847. Thus, $\alpha=\beta/n$=0.017 MPa^{-1}.

The relationship between $\partial\ln\dot{\varepsilon}$ and $\partial(1/T)$ is described by Eq. (15). At a constant temperature T, for $\left[\frac{\partial\ln\dot{\varepsilon}}{\partial\{\ln[\sinh(\alpha\sigma)]\}}\right]_T$, the average slope of seven curves in Fig. 3(c) is obtained to be 5.93904. At constant strain rate $\dot{\varepsilon}$, for $\left[\frac{\partial(1/T)}{\partial\{\ln[\sinh(\alpha\sigma)]\}}\right]_{\dot{\varepsilon}}$, the average slope of four curves in Fig. 3(d) is obtained to be 0.000163. Eventually, the macroscopic activation energy Q is calculated to be 303.8 kJ/mol by Eq. (16).

$$\frac{\partial\ln\dot{\varepsilon}}{\partial(1/T)}=\frac{Q}{R}=\left[\frac{\partial\ln\dot{\varepsilon}}{\partial\{\ln[\sinh(\alpha\sigma)]\}}\right]_T\Big/\left[\frac{\partial(1/T)}{\partial\{\ln[\sinh(\alpha\sigma)]\}}\right]_{\dot{\varepsilon}} \tag{15}$$

$$Q=R\left[\frac{\partial\ln\dot{\varepsilon}}{\partial\{\ln[\sinh(\alpha\sigma)]\}}\right]_T\Big/\left[\frac{\partial(1/T)}{\partial\{\ln[\sinh(\alpha\sigma)]\}}\right]_{\dot{\varepsilon}} \tag{16}$$

Equation (14) is used to perform the fitting analysis. It is possible to obtain the expression of peak stress σ_p as

$$\ln[\sinh(0.017009387\sigma_p)]=\frac{\ln Z-34.38327}{6.31637} \tag{17}$$

4.2 Strain hardening and softening

In general, in the calculation of the strain hardening rate θ, the right side of Eq. (2) is approximately equal to $\Delta\sigma/\Delta\varepsilon$, and the fluctuation of the actual test data has a relatively great impact on the calculation accuracy. Herein, the relationship between the flow stress and strain established by Eq. (11) is subjected to derivative processing, as shown in Eqs. (18) and (19). By incorporating them with Eqs. (4) and (5), we can get the strain hardening rate θ and $-\mathrm{d}\theta/\mathrm{d}\sigma$.

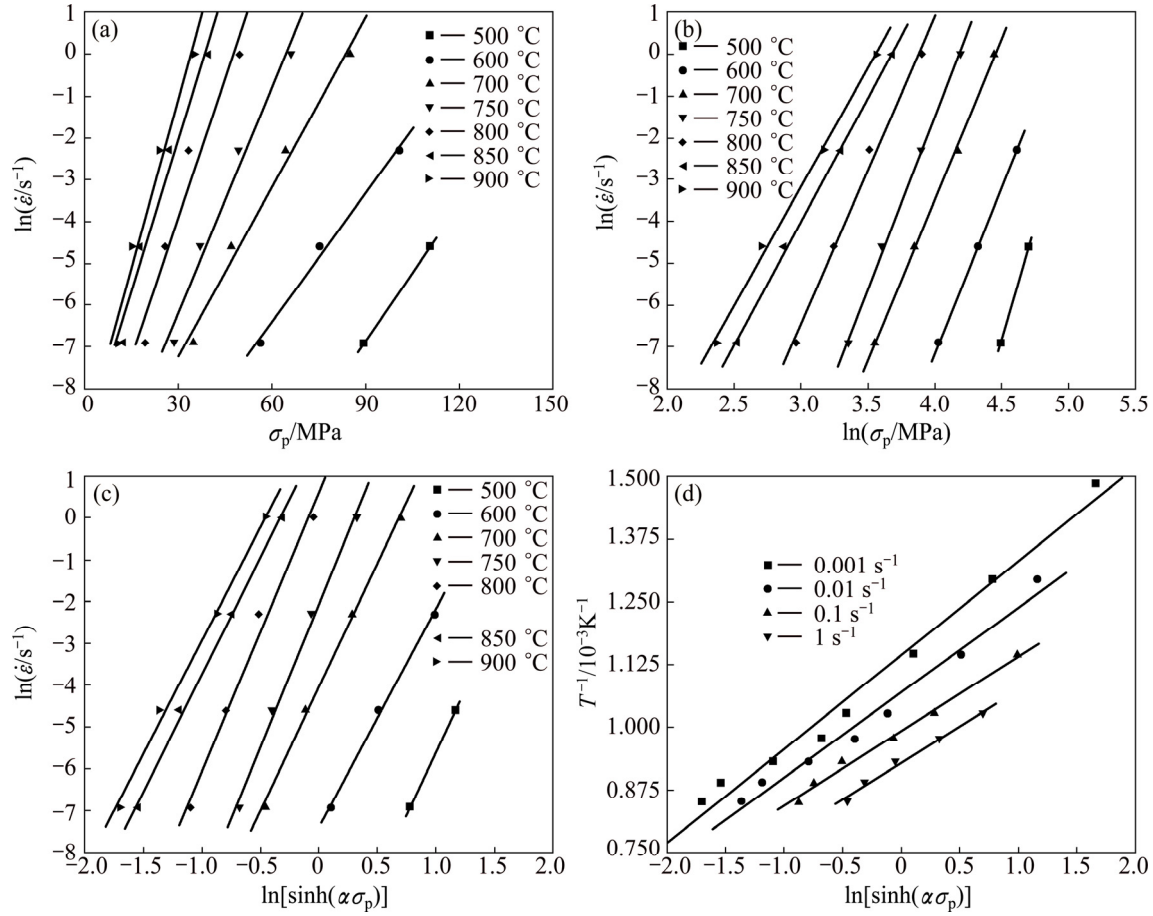

Fig. 3 Relationship between $\ln\dot{\varepsilon}$ and σ_p (a), $\ln\dot{\varepsilon}$ and $\ln\sigma_p$ (b), $\ln\dot{\varepsilon}$ and $\ln[\sinh(\alpha\sigma_p)]$ (c) and T^{-1} and $\ln[\sinh(\alpha\sigma_p)]$ (d)

$$\frac{\mathrm{d}\ln\sigma}{\mathrm{d}\varepsilon}=a_1+\frac{a_2}{\varepsilon}+a_3(\ln\varepsilon+1)+a_4(2\varepsilon\ln\varepsilon+\varepsilon)+a_5[(\ln\varepsilon)^2+2\ln\varepsilon]+2\varepsilon a_6+\frac{2a_7\ln\varepsilon}{\varepsilon}+3\varepsilon^2a_8+\frac{a_9 3(\ln\varepsilon)^2}{\varepsilon} \tag{18}$$

$$\mathrm{d}\left(\frac{\mathrm{d}\ln\sigma}{\mathrm{d}\varepsilon}\right)/\mathrm{d}\varepsilon=-\frac{a_2}{\varepsilon^2}+\frac{a_3}{\varepsilon}+a_4(2\ln\varepsilon+3)+2a_5\left(\frac{\ln\varepsilon+1}{\varepsilon}\right)+2a_6+2a_7\left(\frac{1-\ln\varepsilon}{\varepsilon^2}\right)+6a_8\varepsilon+3a_9\left[\frac{2\ln\varepsilon-(\ln\varepsilon)^2}{\varepsilon^2}\right] \tag{19}$$

where a_1−a_9 are coefficients.

Figure 4 shows the curves of the strain hardening rate θ and the strain ε, from which we can see that the θ value decreases gradually as ε increases. The strain at θ=0 is just the peak strain ε_p. Then, as ε increases, θ value is gradually restored to 0 again. This exhibits an obvious feature of peak value on the flow stress curve, indicating that a discontinuous dynamic recrystallization occurs in this stage. The strain at which θ value returns to 0 for the first time is precisely the steady strain ε_{ss}. This shows that it is now in the state of full dynamic recrystallization. When further increasing the strain, θ value increases again gradually, indicating that the secondary strain hardening is dominant. Accompanying with the increased deformation rate and dropped deformation temperature, the dislocation cross slip and climbing cannot be fully conducted, softening degree provided by the cross slip and climbing is relatively small, rendering the delayed occurrence of peak strain ε_p. At a deformation temperature of 600 °C and a strain rate of 1 s^{-1}, θ value is larger than 0 all the time, indicating that the strain fails to reach the peak strain ε_p. In this stage, the strain hardening exceeds dynamic recovery and dynamic recrystallization softening.

The curves of strain hardening rate θ and stress σ are shown in Fig. 5, which can be divided into four stages. Stage I was a linear hardening stage, starting from the strain initiation until the commencement of subgrain formation. Consequently, the dynamic recovery rate became slow. The slope of the curve turned to be lowered gradually, and the deformation entered into the second linear hardening stage (Stage II). When the deformation reached the critical strain ε_c of a dynamic recrystallization, the strain hardening rate θ quickly dropped to 0 in Stage III. After the strain hardening rate θ

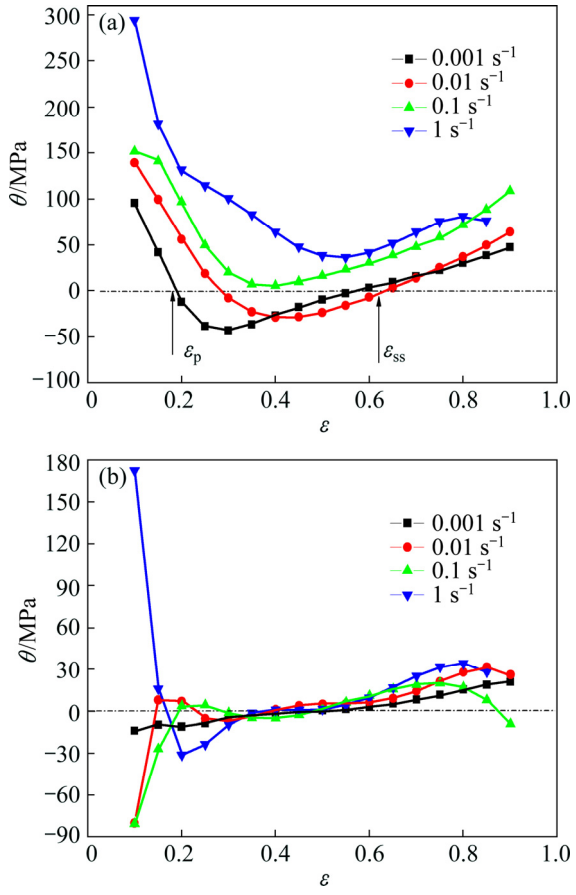

Fig. 4 Curves of strain hardening rate θ vs strain ε at 600 °C (a) and 800 °C (b)

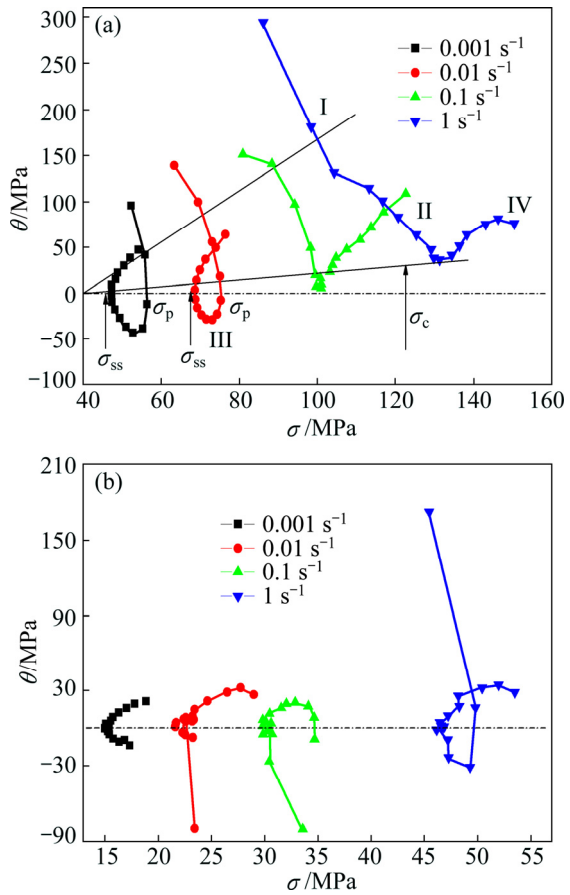

Fig. 5 Curves of strain hardening rate θ vs stress σ at 600 °C (a) and 800 °C (b)

returned to 0 for the first time, θ value increased gradually again with increasing the deformation in Stage IV. Critical stress σ_c could be determined through the inflection point on θ vs σ curve or the minimum value on $(-\mathrm{d}\theta/\mathrm{d}\sigma)$ vs σ curve. The strain corresponding to σ_c value was just the critical strain ε_c, which became larger with the increase of the deformation rate. The critical strain ε_c decreased gradually with the elevation of the deformation temperature. θ value was reduced gradually with the increment of the deformation degree. The stress at θ=0 was just the peak stress value of σ_p. The strain at which θ value returned to 0 for the first time was the steady state stress σ_{ss}. This result is in line with the analytic result shown in Fig. 4. At a deformation temperature of 800 °C and a strain rate of 0.001 s^{-1}, θ value recovered gradually from negative to 0. There was slight difference between the peak stress σ_p and the steady state stress σ_{ss} on the flow stress curve, indicating that the critical strain ε_c required to drive the dynamic recrystallization is relatively small at higher deformation temperatures and lower strain rates. In this stage, the continuous dynamic recrystallization is dominant in terms of the softening mechanism.

Figure 6 show the relationship between the peak strain ε_p and the critical strain ε_c with the parameter Z. Through regression analysis of the calculated $\varepsilon_c/\varepsilon_p$=0.4−0.6, the expression of the peak strain ε_p and the critical strain ε_c could be obtained, respectively, through Eq. (20) and Eq. (21), being close to the lower limit of empirical formula $\varepsilon_c/\varepsilon_p$=0.6−0.85.

$$\varepsilon_p = 0.000242854Z^{0.19521} \tag{20}$$

$$\varepsilon_c = 0.007665772Z^{0.08907} \tag{21}$$

To calculate the σ_{rec} value of Eq. (1), it is needed to further determine σ_{sat}, σ_0 and r values, where, 2% of the total strain is obtained as the initial yield strain ε_0. The initial yield stress σ_0 can be obtained correspondingly. Using Eq. (1), Eq. (22) can be obtained. By incorporating Eqs. (1) and (22) to obtain Eq. (23) to seek derivatives of σ_{rec} and ε:

$$\frac{\mathrm{d}\sigma_{rec}}{\mathrm{d}\varepsilon} = \frac{1}{2}\frac{1}{\sigma_{rec}} r(\sigma_{sat}^2 - \sigma_0^2)\exp[-r(\varepsilon - \varepsilon_0)] \tag{22}$$

$$\frac{\mathrm{d}\sigma_{rec}}{\mathrm{d}\varepsilon}\sigma_{rec} = \frac{r}{2}(\sigma_{sat}^2 - \sigma_{rec}^2) \tag{23}$$

When the strain ε is smaller than the dynamic recrystallization critical strain ε_c, $\mathrm{d}\sigma_{rec}/\mathrm{d}\varepsilon=\theta$. Thus, Eq. (23) can be derived to

$$\theta\sigma_{rec} = \frac{r}{2}(\sigma_{sat}^2 - \sigma_{rec}^2) \tag{24}$$

$$\frac{\mathrm{d}(\theta\sigma_{rec})}{\mathrm{d}\sigma_{rec}^2} = -\frac{r}{2} \tag{25}$$

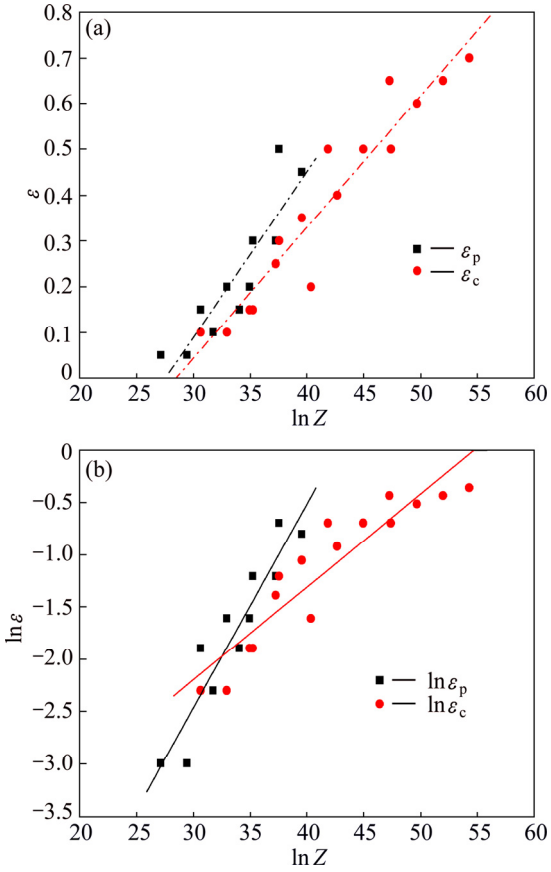

Fig. 6 Relationship between ε_p (ε_c) and ln Z (a) and ln ε_p (ln ε_c) and ln Z (b)

It can be seen from Fig. 7 that σ_{rec}^2 and $\theta\sigma_{rec}$ have a linear relationship. Through the linear regression analysis, the slope (m) of σ_{rec}^2 vs $\theta\sigma_{rec}$ curve is obtained. From Eq. (25), r=−2m is deduced. By extending σ_{rec}^2 and $\theta\sigma_{rec}$ curves to $\theta\sigma_{rec}$ =0, the stress σ_{sat} (location indicated by arrow in Fig. 7) can be saturated.

The determined σ_{sat}, σ_0 and r values are substituted into Eq. (1) for computation. Then, the dynamic recovery stress curve σ_{rec} is available, as shown in Fig. 8. Because the effect of the secondary strain hardening is not taken into account in Eq. (1), the σ_{rec} value gradually approaches the saturated stress σ_{sat} when the strain ε reaches the peak strain ε_p.

To further get the dynamic recovery volume fraction X_{rec} and the dynamic recrystallization volume fraction X_{drx}, it is easily known from Eq. (1) that:

$$\frac{\sigma_{rec}^2 - \sigma_0^2}{\sigma_{sat}^2 - \sigma_0^2} = 1 - \exp[-r(\varepsilon - \varepsilon_0)] \tag{26}$$

For a constant strain rate $\dot{\varepsilon}$, Eq. (26) can be rewritten as

$$X_{rec} = \frac{\sigma_{rec}^2 - \sigma_0^2}{\sigma_{sat}^2 - \sigma_0^2} = 1 - \exp[-r\dot{\varepsilon}(t - \tau)] \tag{27}$$

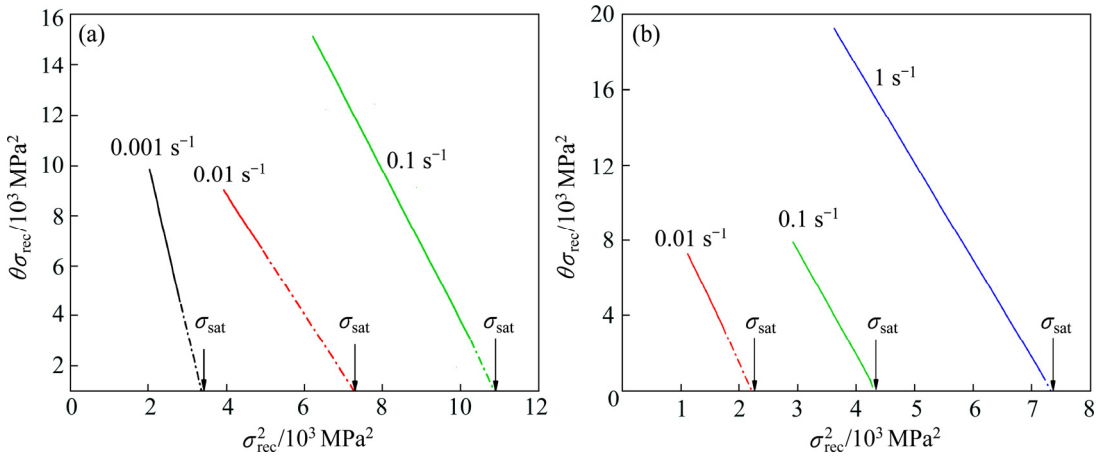

Fig. 7 Relationship between θ and σ at temperatures of 600 °C (a) and 700 °C (b)

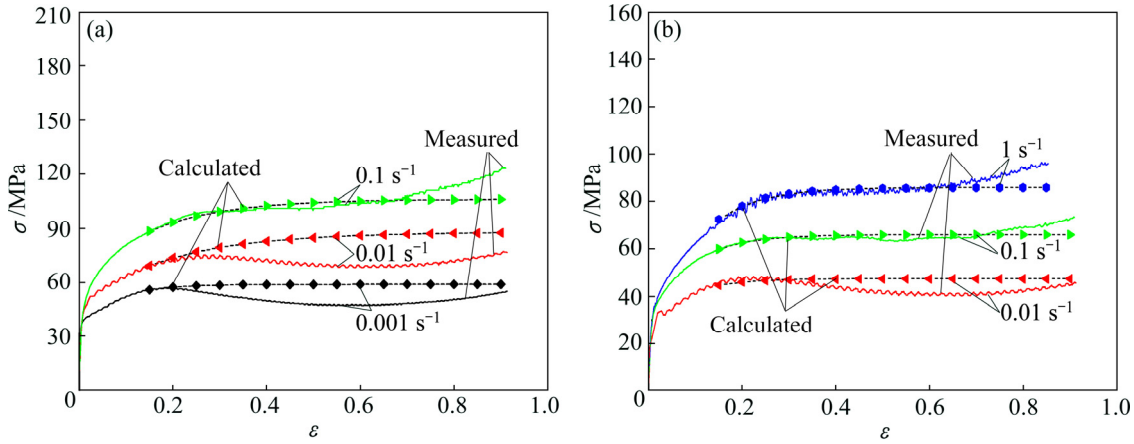

Fig. 8 Comparison between actually measured and calculated σ–ε curves at temperatures of 600 °C (a) and 700 °C (b)

$$\frac{dX_{rec}}{dt} = r\dot{\varepsilon}(1-X_{rec}) \tag{28}$$

where t is the unloading time, τ is the time at which the related phenomenon is initiated (τ is negligible since DRV starts immediately after straining). At a constant strain rate $\dot{\varepsilon}$, dX_{rec}/dt increases when r increases. Therefore, the physical meaning of r lies in constructing a bridge between the dynamic recovery kinetics and the deformation conditions.

After the deformation reaches the critical strain ε_c, dynamic recrystallization volume fraction X_{drx} can be expressed using the Avrami equation [11−13]:

$$X_{drx} = 1-\exp\left[k\left(\frac{t}{t_{0.5}}\right)^n\right] \tag{29}$$

where k is the coefficient related to deformation conditions with the value equal to $\ln(1-X_{drx})$, when the dynamic recrystallization volume fraction is 50%, k=−0.693. n is the time exponent, and n=2 is taken; t is the unloading time; $t_{0.5}$ is the time when the dynamic recrystallization volume fraction is 50%. As the rates of the nucleation and the grain growth during the dynamic recrystallization are not constant, the crystal nucleus is also not the homogeneous nucleation in the whole volume. According to the theory of recrystallization and model structure [11], we can obtain

$$X_{drx} = 1-\exp\left[-0.693\left(\frac{\varepsilon-\varepsilon_c}{\varepsilon_{0.5}-\varepsilon_c}\right)^2\right] \tag{30}$$

$$\varepsilon_{0.5} = \frac{\varepsilon_{ss}+\varepsilon_c}{2} \tag{31}$$

From Fig. 2, the difference between σ_{rec} and σ_{drx} can be represented as $\Delta\sigma$, which is the net softening directly attributed to DRX. Then, the softening fraction due to DRX can be prescribed by Eq. (32). Meanwhile, after incorporating with Eq. (30), the dynamic recrystallization stress curve σ_{drx} can be achieved:

$$X_{drx} = \frac{\Delta\sigma}{\sigma_{sat}-\sigma_{ss}} = \frac{\sigma_{rec}-\sigma_{drx}}{\sigma_{sat}-\sigma_{ss}} \tag{32}$$

$$\sigma_{drx} = \sigma_{rec}-(\sigma_{sat}-\sigma_{ss})\left\{1-\exp\left[-0.693\left(\frac{\varepsilon-\varepsilon_c}{\varepsilon_{0.5}-\varepsilon_c}\right)^2\right]\right\} \tag{33}$$

Figure 9(a) shows the dynamic recovery volume fraction X_{rec} of the material at a deformation temperature of 700 °C. The X_{rec} value increases sharply as the strain increases. After it reaches the critical strain ε_c, X_{rec} value increases slowly. As the strain reaches 0.5, the material is basically in a state of full dynamic recovery. Figure 9(b) shows the dynamic recrystallization volume fraction X_{drx} of the material at a deformation temperature of 600 °C. The X_{drx} value increases rapidly after the deformation reaches the critical strain ε_c, and tends to 1 when the strain reaches a steady state strain ε_{ss}, getting in a state of full dynamic recrystallization. With further increasing strain, the effect of secondary hardening is strengthened, exceeding the dynamic recrystallization softening with a rapidly decreased X_{drx}. With increasing strain rate and decreasing temperature, the dislocation density increases, and in turn higher deformation activation energy is required to drive dynamic recovery and dynamic recrystallization [2,26]. This results in the reduction of X_{rec} and X_{drx} values.

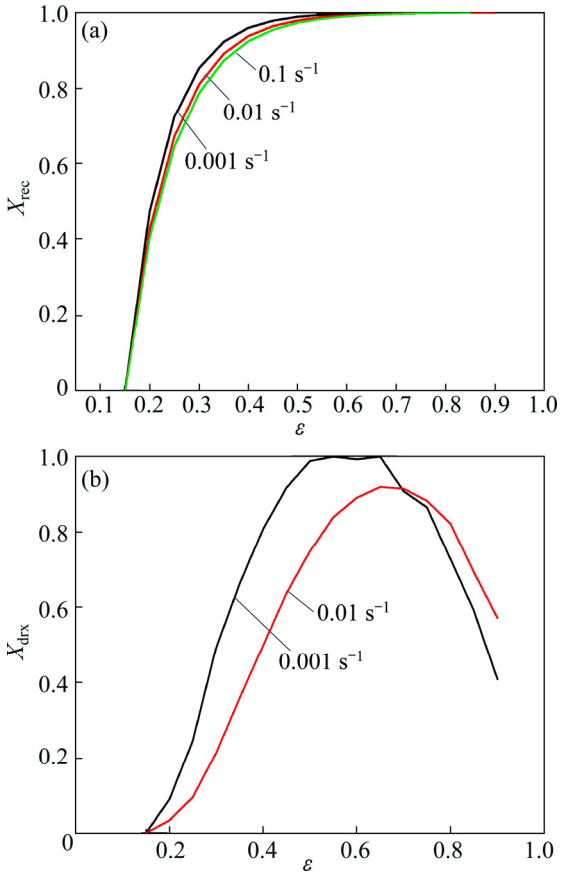

Fig. 9 Relationships between dynamic recovery volume fraction and true strain at 700 °C (a) and true strain dynamic recrystallization volume fraction and true strain at 600 °C (b)

4.3 Processing map

Figure 10 shows the processing map of the pure copper at a strain of 0.6. The contour numbers represent the efficiency of dissipation, and the red region corresponds to the flow instability in Fig. 10. It can be seen that there is a large region that corresponds to a feasible processing window, and only one flow instability region can be observed, which occurs in low temperature and high strain rate region (400−450 °C, 0.001−0.05 s^{-1} and 450−750 °C, 0.05−1 s^{-1}). Instability mechanisms are likely associated with cracking, localized plastic flow and adiabatic shear bands. Figure 11 shows the optical microstructure of the pure copper in the stability region. It can be seen that many dynamic recrystallization grains can be observed, which suggests that the deformation mechanism in the stability region is dynamic recrystallization.

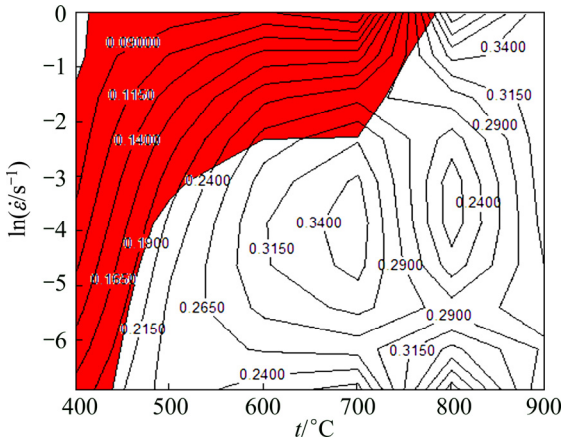

Fig. 10 Processing map of pure copper at strain of 0.6

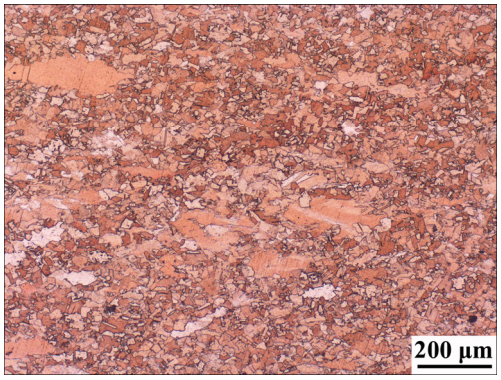

Fig. 11 Microstructure under condition of 600 °C and 0.01 s^{-1}

5 Conclusions

1) With increasing deformation degree, the hot compression deformation of pure copper exhibits features including strain hardening and softening. Before the deformation degree reaches the critical strain, strain hardening and dynamic recovery dominate the deformation, and the flow stress increases significantly. After the deformation degree exceeds the peak strain, the dynamic recrystallization softening enables the flow stress to decrease gradually.

2) The true stress–true strain curves predicted by the

extracted model are in good agreement with the experimental results. The expression of strain hardening rate, dynamic recrystallization critical stress, saturated stress, dynamic recovery volume fraction and dynamic recrystallization volume fraction are determined.

3) The peak value feature on the flow stress curve is unable to uniquely characterize the dynamic recrystallization softening behavior. The expressions of the dynamic recrystallization critical strain and the peak strain with parameter Z are established, respectively. The critical strain increases when the value of parameter Z increases. There is a certain correlation between the critical strain and the peak strain that can be expressed as $\varepsilon_c/\varepsilon_p$=0.4−0.6.

4) According to the processing map established, the instability region occurs in regions of 400−450 °C, 0.001−0.05 s^{-1} and 450−750 °C, 0.05−1 s^{-1}. The deformation mechanism in the stability region is dynamic recrystallization.

References

[1] CHANDLER H D. Work hardening characteristics of copper from constant strain rate and stress relaxation testing [J]. Materials Science and Engineering A, 2009, 506: 130−134.

[2] ZHU An-yin, CHEN Jing-lin, LI Zhou, LUO Li-yang, LEI Qian, ZHANG Liang, ZHANG Wan. Hot deformation behavior of novel imitation-gold copper alloy [J]. Transactions of Nonferrous Metals Society of China, 2013, 23(4): 1349−1355.

[3] PRASAD Y V R K, RAO K P. Influence of oxygen on rate-controlling mechanisms in hot deformation of polycrystalline copper: Oxygen-free versus electrolytic grades [J]. Materials Letters, 2004, 58: 2061−2066.

[4] ROKNI M R, ZAREI-HANZAKI A, ROOSTAEI A A, ABOLHASANI A. Constitutive base analysis of a 7075 aluminum alloy during hot compression testing [J]. Materials and Design, 2011, 32: 4955−4960.

[5] XIA Xiang-sheng, CHEN Qiang, ZHANG Kui, ZHAO Zu-de, MA Ming-long, LI Xing-gang, LI Yong-jun. Hot deformation behavior and processing map of coarse-grained Mg–Gd–Y–Nd–Zr alloy [J]. Materials Science and Engineering A, 2013, 587: 283−290.

[6] CHEN Qiang, ZHAO Zu-de, CHEN Gang, WANG Bo. Effect of accumulative plastic deformation on generation of spheroidal structure, thixoformability and mechanical properties of large-size AM60 magnesium alloy [J]. Journal of Alloys and Compounds, 2015, 632: 190−200.

[7] PENG Wen-wen, ZENG Wei-dong, WANG Qing-jiang, ZHAO Qin-yang, YU Han-qing. Effect of processing parameters on hot deformation behavior and microstructural evolution during hot compression of as-cast Ti60 titanium alloy [J]. Materials Science and Engineering A, 2014, 593: 16−23.

[8] GRONOSTAJSKI Z. A general model describing flow stress of copper alloys in different deformation conditions [J]. Journal of Materials Processing Technology, 2003, 142: 684−691.

[9] MANONUKUL A, DUNNE F P E. Initiation of dynamic recrystallization under inhomogeneous stress states in pure copper [J]. Acta Materialia, 1999, 47: 4339−4354.

[10] PRASAD Y V R K, RAO K P. Mechanisms of high temperature deformation in electrolytic copper in extended ranges of temperature and strain rate [J]. Materials Science and Engineering A, 2004, 374: 335−341.

[11] WANG L, LIU F, ZUO Q, CHEN C F. Prediction of flow stress for N08028 alloy under hot working conditions [J]. Materials and Design, 2013, 47: 737−745.

[12] LIANG Hou-quan, GUO Hong-zhen, NING Yong-quan, PENG Xiao-na, QIN Chun, SHI Zhi-feng, NAN Yang. Dynamic recrystallization behavior of Ti−5Al−5Mo−5V−1Cr−1Fe alloy [J]. Materials and Design, 2014, 63: 798−804.

[13] MOSTAFAEI M A, KAZEMINEZHAD M. A novel approach to find the kinetics of dynamic recovery based on hot flow curves [J]. Materials Science and Engineering A, 2012, 544: 88−91.

[14] XIA Xiang-sheng, CHEN Qiang, LI Jian-ping, SHU Da-yu, HU Chuan-kai, HUANG Shu-hai, ZHAO Zu-de. Characterization of hot deformation behavior of as-extruded Mg−Gd−Y−Zn−Zr alloy [J]. Journal of Alloys and Compounds, 2014, 610: 203−211.

[15] PUCHI-CABRERA E S, STAIA M H, GUÉRIN J D, LESAGE J, DUBAR M, CHICOT D. An experimental analysis and modeling of the work-softening transient due to dynamic recrystallization [J]. International Journal of Plasticity, 2014, 54: 113−131.

[16] LI Xiao-cheng, DUAN Li-li, LI Jun-wan, WU Xiao-chun. Experimental study and numerical simulation of dynamic recrystallization behavior of a micro-alloyed plastic mold steel [J]. Materials and Design, 2015, 66: 309−320.

[17] LIU Yan-xing, LIN Yong-cheng, LI Hong-bin, WEN Dong-xu, CHEN Xiao-min, CHEN Ming-song. Study of dynamic recrystallization in a Ni-based superalloy by experiments and cellular automaton model [J]. Materials Science and Engineering A, 2015, 626: 432−440.

[18] LUO Shou-jing, CHEN Qiang, ZHAO Zu-de. An investigation of microstructure evolution of RAP processed ZK60 magnesium alloy [J]. Materials Science and Engineering A, 2009, 501: 146−152.

[19] CHEN Qiang, LUO Shou-jing, ZHAO Zu-de. Microstructural evolution of previously deformed AZ91D magnesium alloy during partial remelting [J]. Journal of Alloys and Compounds, 2009, 477: 726−731.

[20] MENG Gang, LI Bo-long, LI Hong-mei, HUANG Hui, NIE Zuo-ren. Hot deformation and processing maps of an Al−5.7 wt.%Mg alloy with erbium [J]. Materials Science and Engineering A, 2009, 517: 132−137.

[21] PRASAD Y V R K, RAO K P. Effect of homogenization on the hot deformation behavior of cast AZ31 magnesium alloy [J]. Materials and Design, 2009, 30: 3723−3730.

[22] MIRZADEH H, NAJAFIZADEH A. Flow stress prediction at hot working conditions [J]. Materials Science and Engineering A, 2010, 527: 1160−1164.

[23] SERAJZADEH S, TAHERI A K. Prediction of flow stress at hot working condition [J]. Mechanics Research Communications, 2003, 30: 87−93.

[24] ZAFIR-ALAM M, KAMAT S V, JAYARAM V, KARAMCHED P S, GHOSAL P, DAS D K. Dynamic recovery and recrystallization during high-temperature tensile deformation of a free-standing Pt-aluminide bond coat [J]. Materials Science and Engineering A, 2014, 604: 18−22.

[25] LI Luo-xing, WANG Guan, LIU Jie, YAO Zai-qi. Flow softening behavior and microstructure evolution of Al−5Zn−2Mg aluminum alloy during dynamic recovery [J]. Transactions of Nonferrous Metals Society of China, 2014, 24(1): 42−48.

[26] LIU Na, LI Zhou, LI Ling, LIU Bin, XU Gen-ying. Processing map and hot deformation mechanism of novel nickel-free white copper alloy [J]. Transactions of Nonferrous Metals Society of China, 2014, 24(11): 3492−3499.

应变速率和变形温度对纯铜应变硬化和软化行为的影响

黄树海，舒大禹，胡传凯，朱世凤

西南技术工程研究所，重庆 400039

摘　要：通过热压缩实验研究变形温度和应变速率对纯铜热变形行为的影响，确定了应变硬化率、动态再结晶临界应力、饱和应力、动态回复体积分数和动态再结晶体积分数的表达式。结合热加工图，得到纯铜的失稳区域主要位于 400~450 °C、0.001~0.05 s^{-1} 和 450~750 °C、0.05~1 s^{-1} 区间，稳态区域的变形机制主要为动态再结晶。对流变应力进行预测，预测结果与实验结果吻合较好。

关键词：铜；热压缩变形；应变硬化；应变软化

(Edited by Wei-ping CHEN)